ACCOUNTS
of chemical research

The Spectral Signatures of Frenkel Polarons in H- and J-Aggregates

FRANK C. SPANO*
Department of Chemistry, Temple University, Philadelphia, Pennsylvania 19122

RECEIVED ON AUGUST 25, 2009

CONSPECTUS

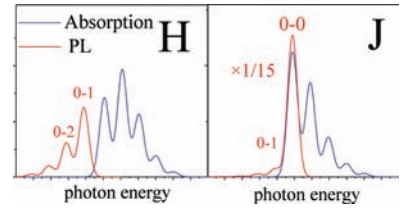

Electronic excitations in small aggregates, thin films, and crystals of conjugated organic molecules play a fundamental role in the operation of a wide array of organic-based devices including solar cells, transistors, and light-emitting diodes. Such excitations, or excitons, are generally spread out over several molecules: a balance between the delocalizing influence of resonant intermolecular coupling and the localizing influence of static and dynamic disorder determines the coherence range of the exciton. Because of the "soft" nature of organic materials, significant nuclear relaxation in the participating molecules also accompanies the electronic excitations. To properly understand energy or charge transport, one must treat intermolecular (excitonic) coupling, electron-vibrational coupling, and disorder on equal footing. In this Account, we review the key elements of a theoretical approach based on a multiparticle representation that describes electronic excitations in organic materials as vibronic excitations surrounded by a field of vibrational excitations. Such composite excitations are appropriately called Frenkel excitonic polarons.

For many conjugated molecules, the bulk of the nuclear reorganization energy following electronic excitation arises from the elongation of a symmetric vinyl stretching mode with energy $\sim$1400 cm^{-1}. To appreciate the impact of aggregation, we study how the vibronic progression of this mode, which dominates the isolated (solvated) molecule absorption and emission spectra, is distorted when molecules are close enough to interact with each other. As we demonstrate in this Account, the nature of the distortion provides a wealth of information about how the molecules are packed, the strength of the excitonic interactions between molecules, the number of molecules that are coherently coupled, and the nature of the disorder. We show that the aggregation-induced deviations from the Poissonian distribution of vibronic peak intensities take on two extremes identified with ideal H- and J-aggregates.

The sign of the nearest neighbor electronic coupling, positive for H and negative for J, distinguishes the two basic aggregate forms. For several decades, researchers have known that H-aggregates exhibit blue-shifted absorption spectra and are subradiant while J-aggregates exhibit the opposite behavior (red-shifted absorption and superradiance). However, the exact inclusion of exciton−vibrational coupling reveals several more distinguishing traits between the two aggregate types: in H(J)-aggregates the ratio of the first two vibronic peak intensities in the absorption spectrum decreases (increases) with increasing excitonic coupling, while the ratio of the 0−0 to 0−1 emission intensities increases (decreases) with disorder and increases (decreases) with increasing temperature. These two extreme behaviors provide the framework for understanding absorption and emission in more complex morphologies, such as herringbone packing in oligo(phenylene vinylene)s, oligothiophenes and polyacene crystals, as well as the polymorphic packing arrangements observed in carotenoids.

I. Introduction

Electronic excitations in organic aggregates, films, and crystals continues to be an area of significant current interest driven mainly by promising commercial applications including light-emitting diodes and solar cells.[1−4] Unlike their inorganic counterparts, organic semiconductors are soft in the sense that energy and charge transport are accompanied by significant nuclear rearrangements. Optical excitations are therefore composite particles involving electronic and vibrational degrees of freedom.[5−7]

The absorption and emission spectra of a great many conjugated molecules reveal a vibronic progression arising from a symmetric vinyl stretch-

Published on the Web 12/16/2009 www.pubs.acs.org/acr
10.1021/ar900233v

ing mode (or closely spaced cluster of modes) with energy ~1400 cm^{-1}. Elongation along the mode coordinate subsequent to $S_0 \rightarrow S_1$ optical excitation is responsible for a nuclear reorganization energy of ~0.2 eV. Recently, several theoretical approaches have been advanced to better understand the impact of exciton−vibrational coupling involving the 1400 cm^{-1} mode on the optical response.[8−16] By appreciating how the Franck−Condon (FC) progression is distorted in going from the isolated molecule to a molecular assembly one can derive important information about molecular packing, the exciton bandwidth, the nature of disorder and the exciton coherence length. In addition, one can probe the structure of the fundamental excitations responsible for absorption and emission. Particularly useful in this respect is the multiparticle basis set originally introduced by Philpott.[17] The basis set allows one to obtain essentially exact steady-state absorption and emission spectral profiles using a Holstein-like Hamiltonian[7] to represent exciton−vibrational coupling.

From a purely electronic perspective, the impact of molecular aggregation on the optical response was worked out early on by Kasha.[18,19] When the sign of the resonant electronic (excitonic) coupling is positive,[20] as for a pair of rod-shaped molecules in a side-by-side orientation, the main absorption peak shifts to higher energies and fluorescence is quenched.[21,22] These are the so-called H-aggregates. In J-aggregates the couplings are negative, resulting in a spectral red shift.[23] J-aggregates occur when "head-to-tail" orientations dominate and can be superradiant at low temperatures.[24]

When vibronic coupling is included the resulting FC progressions characterizing absorption and emission are affected differently by J- and H-aggregation. The contrasting ways in which the progressions are distorted away from a Poissonian distribution in these extreme aggregate types is the subject of this Account. Although more complex morphologies such as those based on unit cells with more than one molecule cannot be classified as purely H or J their optical properties can nevertheless be understood within the framework of the ideal aggregate types. Examples include the optical responses of a wide range of organic materials including aggregates or thin films of poly(3-hexyl thiophene) or P3HT,[25−27] oligo(phenylene vinylene)s and oligothiophenes,[21,22,28] polyacenes,[29,30] and carotenoids.[31,32]

II. Excitonic Polarons

Excitations in organic materials are Frenkel excitons (or excitonic polarons) comprised of a vibronically excited central molecule surrounded by vibrationally, but not electronically, excited molecules. The latter are geometrically distorted, due to elongation along one (or more) symmetric vibrational coordinate(s). The situation is analogous to a bowling ball on a mattress as shown in Figure 1. The ball and the spring directly underneath correspond to the vibronically excited molecule, while the neighboring springs correspond to the surrounding vibrationally excited molecules. As the bowling ball traverses the mattress, the compression field of the underlying springs travels with it, in exact analogy to the Frenkel polaron considered here (with the exception that excited molecules are elongated and not compressed along the vibrational coordinate.) Delocalization loosely corresponds to the range over which the ball travels.

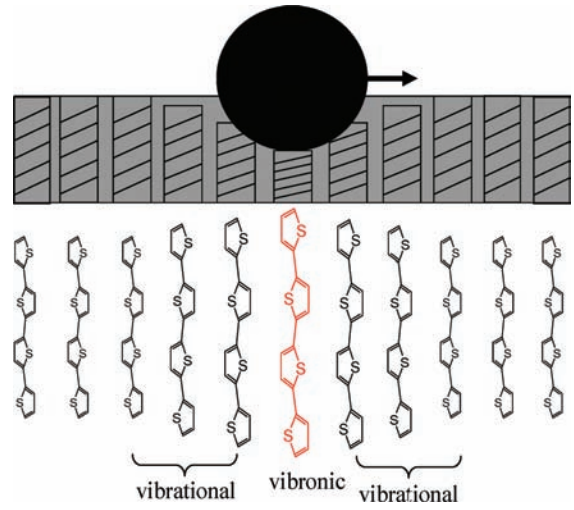

FIGURE 1. Analogy of the motion of a Frenkel polaron in a linear aggregate with a bowling ball on a mattress.

In order to account quantitatively for exciton−vibrational coupling, we have assumed a simple model in which the nuclear potentials corresponding to the ground (S_0) and electronically excited (S_1) molecular states are shifted harmonic wells of identical frequency, ω_0. The shift is quantified by the Huang−Rhys (HR) factor, λ^2, which is approximately unity for the 1400 cm^{-1} mode. To describe the collective excitations, we employed the multiparticle basis set[9,17] as depicted in Figure 2. A single-particle excitation, $|n,\tilde{v}\rangle$, consists of a vibronically excited chromophore at site n with $\tilde{v}$ excited-state quanta in the S_1 nuclear potential, with all other molecules electronically and vibrationally unexcited. A vibronic/vibrational *pair* excitation, denoted $|n,\tilde{v};n',v'\rangle$, is a two-particle state. In addition to a vibronic excitation at n, this state includes a *vibrational* excitation at n' ($\neq n$) with v'(≥ 1) quanta in the S_0 potential, as demonstrated schematically in Figure 2. Such states are necessary for describing the spatial extent of the vibrational

distortion field surrounding the central vibronic excitation, characterized by the polaron radius. Within the two-particle approximation, the αth eigenstate of the aggregate Hamiltonian can be expanded in one- and two-particle states;

$$|\psi^{(\alpha)}\rangle = \sum_{n,\tilde{v}} c^{(\alpha)}_{n,\tilde{v}} |n,\tilde{v}\rangle + \sum_{n,\tilde{v}} \sum_{n',v'} c^{(\alpha)}_{n,\tilde{v};n'v'} |n,\tilde{v};n',v'\rangle \qquad (1)$$

The above expansion is highly accurate for obtaining the optical response in organic assemblies where the singlet exciton bandwidth ranges from 0 to 1.0 eV and where the nuclear relaxation energy, $\lambda^2\omega_0$, is approximately 0.2 eV. Three-particle contributions have negligible effect on absorption and emission.[9] Hence, we can obtain an essentially exact solution to the polaron's optical response for relatively large aggregates.

The optical response from the excitons in eq 1 derives from the following basic properties: (i) Only one-particle states are optically allowed from the vibrationless ground state. Two-particle states are forbidden via one- (and two-) photon excitation. Hence, only one-particle states contribute to the 0−0 emission. (ii) Both one- and two-particle states radiatively couple to the electronic ground state with one or more vibrational excitations. Thus, sideband emission involves both one- and two-particle states. (iii) When disorder is absent and periodic boundary conditions apply, the exciton wavenumber k becomes a good quantum number. Only nodeless excitons with $k = 0$ can be optically excited from the vibrationless ground state. In J-aggregates, the $k = 0$ exciton resides at the band bottom, while the dark $k = \pi$ exciton with $N - 1$ nodes resides at the top of the band. The order is reversed in H-aggregates.

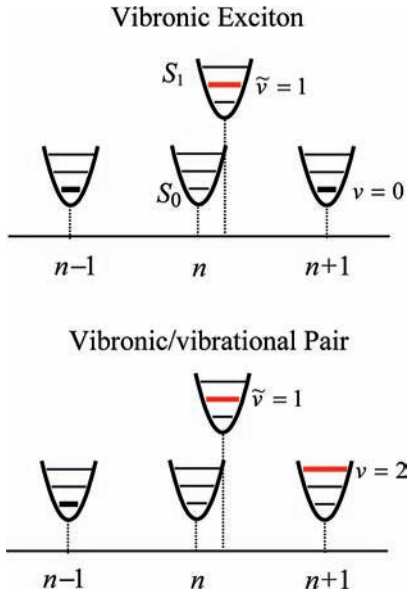

FIGURE 2. Examples of the fundamental excitations in ordered organic assemblies. The vibronic (single-particle) excitation shown is $|n,\tilde{v} = 1\rangle$, while the vibronic/vibrational pair (two-particle state) is $|n,\tilde{v} = 1;n + 1,v = 2\rangle$.

The coefficients involved in the expansion 1 can be evaluated by diagonalizing the aggregate Hamiltonian H. The diagonal elements of H consist of the energies of the localized states: taking $\hbar = 1$, we have $\omega_{0-0} + D + \tilde{v}\omega_0 + \Delta_n$ for the one-particle state, $|n,\tilde{v}\rangle$, and $\omega_{0-0} + D + (\tilde{v} + v')\omega_0 + \Delta_n$ for the two-particle states, $|n,\tilde{v};n',v'\rangle$. Here, ω_{0-0} is the gas-phase 0−0 molecular transition energy corresponding to the lowest optically allowed transition (normally, $S_0 \rightarrow S_1$), D is the gas-to-crystal shift due to nonresonant intermolecular interactions, Δ_n represents a disorder-induced change in the transition energy at site n, and ω_0 is the aforementioned energy of the symmetric intramolecular vibration. The off-diagonal elements of H are represented by the usual excitonic Hamiltonian,

$$H_{ex} = \sum_{m,n} J_{mn} |m\rangle\langle n| \qquad (2)$$

where $|n\rangle$ represents a pure (S_1) electronic excitation at site n (with all other molecules electronically unexcited) and J_{mn} is the excitonic coupling between the mth and nth molecules. The off-diagonal matrix elements of H connecting one-particle states allow for resonant energy transfer in the conventional Frenkel exciton theory. However, H_{ex} also allows for resonant transfer among two-particle states, as well as the coupling between one- and two-particle states (and generally, between n- and $(n+1)$-particle states).[9,17,22] Because of the latter, the one-photon oscillator strength, which is confined entirely to one-particle excitations, becomes increasingly "borrowed" by two-particle states as the excitonic coupling increases and the wave functions take on an increasing mixed one- and two-particle character. All of the aforementioned matrix elements of H_{ex} necessarily involve vibrational overlap integrals, which depend on the HR factor.[11] Finally, the Hamiltonian as described above is exactly equivalent to the Holstein Hamiltonian[7] when the latter is represented in the one- and two-particle basis.

III. Absorption and Emission in Ideal H- and J-Aggregates

In what follows, we consider a linear array of N chromophores (see Figure 1) with nearest neighbor coupling (J_0) only and open boundary conditions. The aggregates are *ideal* in the sense of containing a single molecule per unit cell with no disorder present ($\Delta_n = 0$). Both H- ($J_0 > 0$) and

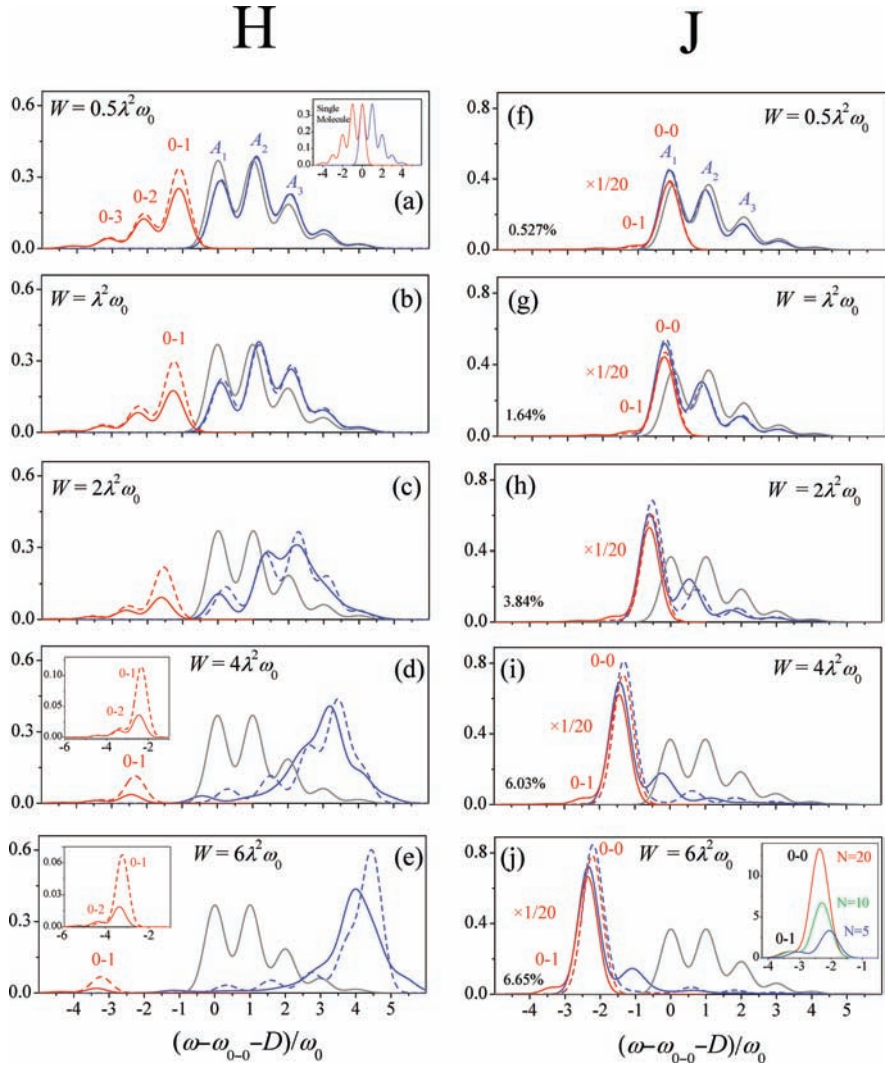

FIGURE 3. Calculated absorption (blue) and emission (red) spectra for linear H- and J-aggregates containing $N = 20$ molecules with nearest-neighbor-only coupling, J_0, and $D = 0$ using eq's (3) and (7). Note the slightly different vertical scales for H and J spectra. In all calculations the values $\sigma_{hom} = 0.4\omega_0$, λ^2 and $\omega_0 = 0.17$ eV (1400 cm^{-1}) were taken. The exciton bandwidth, $W = 4|J_0|$, increases from top to bottom. Solid spectra are evaluated using one- and two-particle states, while dashed spectra use only one-particle states. Inset in panel a shows the isolated-molecule spectra. Gray absorption spectrum appearing in all panels pertains to the isolated molecule ($W = 0$). Insets in panels d and e are enlarged emission spectra. Inset in panel j shows unscaled emission spectrum for different values of N. Number in the lower left corner of panels f−j is the percent admixture of two-particle states in $|em\rangle$, which is identical for J- and H-aggregates with the same W.

J-aggregate ($J_0 < 0$) configurations are considered. We further assume the temperature to be low enough to effectively discount thermally excited emission. Finally, the number of chromophores is chosen to be large enough ($N = 20$) to minimize finite-size effects. The simple aggregates just described are sufficient to understand the most salient manifestations of exciton−phonon coupling in the optical response of aggregates and crystals of a broad array of conjugated molecules and polymers. The important effects of disorder and increasing temperature are taken up in the following section.

We begin with absorption. Figure 3 shows calculated spectra for increasing exciton bandwidth, $W = 4|J_0|$, in H- (a−e) and J-aggregates (f−j), evaluated from the expression

$$A(\omega) = \frac{1}{N\mu^2}\sum_{\alpha} |\langle G|\hat{\mu}|\psi^{(\alpha)}\rangle|^2\Gamma(\omega - \omega^{(\alpha)}) \qquad (3)$$

where μ is the molecular transition dipole moment and the sum runs over all dipole-allowed transitions from the vibrationless ground state $|G\rangle$ to the excitons $|\psi^{(\alpha)}\rangle$ with energies $\omega^{(\alpha)}$. $\Gamma(\omega)$ is the homogeneous line shape function, taken to be

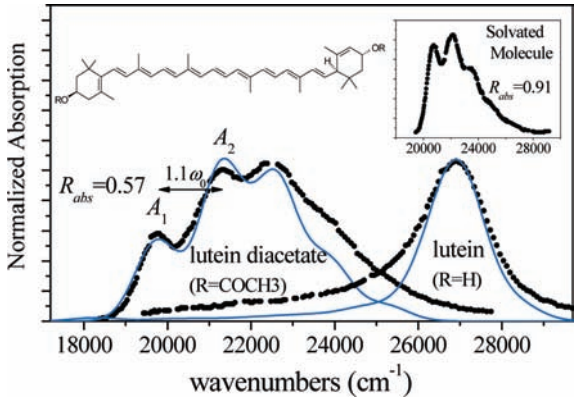

FIGURE 4. Absorption spectra for lutein and lutein diacetate H-aggregates from ref 31 alongside the calculated spectra from ref 32 (blue). Inset shows the spectrum of unaggregated lutein diacetate in acetone. The lutein/acetone spectrum (not shown) is almost identical.

Gaussian, $\Gamma(\omega) = \exp(-\omega^2/\sigma_{hom}^2)$, in Figure 3. The parameters defining *H* are given in the figure caption.

Figure 3 shows spectra calculated from only one-particle states (dashed) and more accurate spectra including one- and two-particle states (solid). We have also calculated spectra with up to three-particle states, but even for the highest *W* in Figure 3, three-particle states contribute only small changes (<5%) to the spectrum.

The isolated-molecule spectrum shown in the inset of Figure 3a consists of a FC progression with the $0-n$ intensity scaling as $\lambda^{2n}\exp(-\lambda^2)/n!$. For the value $\lambda^2 = 1$ used in the figure, the isolated-molecule $0-0$ and $0-1$ peak intensities are therefore equal. In the aggregate absorption spectrum, the peak labeled A_{n+1} correlates to the $0-n$ molecular transition. A_{n+1} is only slightly blue(red)-shifted from the $0-n$ molecular transition in H(J)-aggregates when the exciton coupling is relatively weak ($W < \lambda^2\omega_0$) as in Figure 3a,b,f,g. In this regime, the magnitude of the gas-to-crystal red shift, $|D|$, which is set to zero in Figure 3 in order to focus on excitonic shifts, can easily exceed the exciton blue shift, forcing an overall spectral red shift in an H-aggregate. A similar effect occurs in polymer H-aggregates where a red shift from enhanced molecular planarization overwhelms the smaller excitonic blue shift. Hence, spectral shifts are unreliable for distinguishing H and J aggregation in the weak coupling regime.[32]

As *W* increases in H-aggregates, A_1 diminishes (while the A_3 increases) relative to A_2. Exactly the opposite behavior occurs in J-aggregates. In both aggregates (but more pronounced in H-aggregates), the vibronic peaks become irregularly spaced, with the separation between A_1 and A_2 exceeding ω_0.[32,33] Such aggregation-induced spectral distortions have been observed in P3HT thin films[25−27] and loosely packed carotenoid aggregates[31,32] such as the lutein diacetate H-aggregates shown in Figure 4.

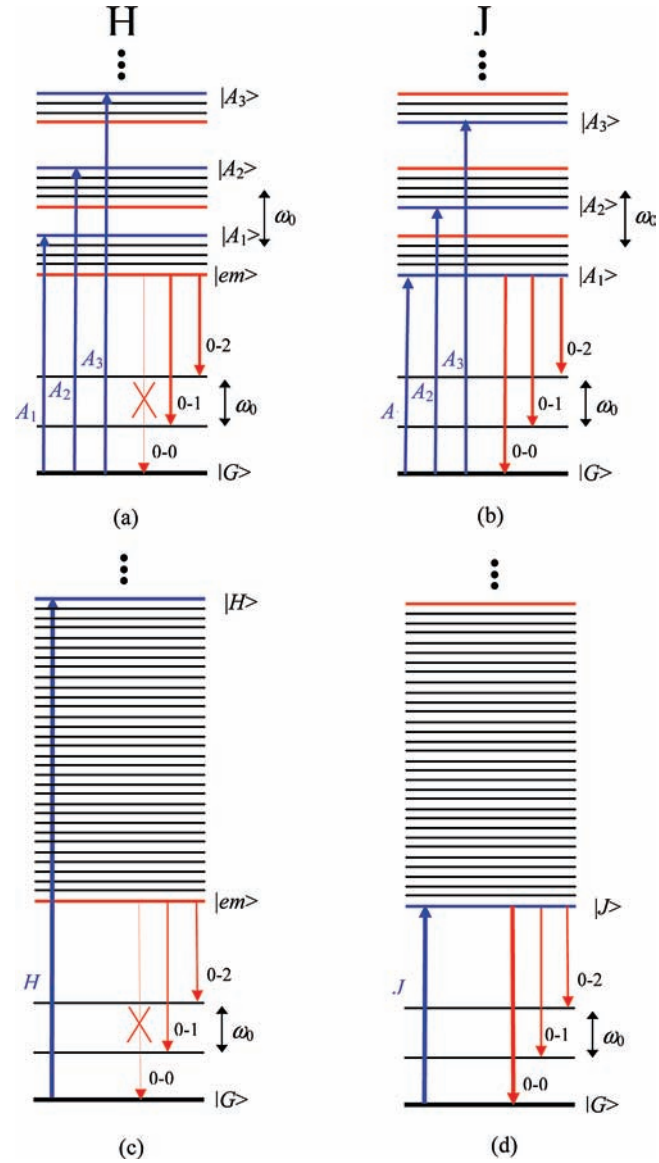

FIGURE 5. Approximate level diagrams corresponding to the weak (a,b) and strong (c,d) exciton coupling regimes in ideal H- and J-aggregates. Blue energy levels correspond to nodeless ($k = 0$) excitons, while red levels are $k = \pi$ excitons. Three and higher phonon states in the ground electronic state are not shown. Note that the bandgap is not to scale.

In the weak excitonic coupling regime, the inclusion of two-particle states has practically no effect on the spectral line shape (Figure 3a,b,f,g) indicating that the states responsible for absorption remain localized (small radius) polarons. However, as *W* increases into the intermediate coupling regime, two-particle states cause significant deviations, indicating the involvement of larger radius polarons. The deviations arise from enhanced one- and two-particle mixing induced by the matrix elements of H_{ex}, which connect one- and two-particle

states. In the strong coupling regime, the absorption spectrum is dominated by an intense blue-shifted (red-shifted) peak in H(J)-aggregates (see Fig. 3e,j). The effect is clearly observed in a variety of cationic dye (J) aggregates[23] and oligo(phenylene vinylene) (OPV) and oligothiophene (OT) H-like aggregates.[21] An additional example of the latter are the lutein H-aggregates in Figure 4, where hydrogen bonding from the terminal OH groups (R = H) induces tighter packing than that found in lutein diacetate aggregates.[31]

The redistribution of oscillator strength toward higher (lower) energy in H(J)-aggregates in the weak coupling regime can be understood from the energy-level diagrams in Figure 5a,b. When H_{ex} is treated as a perturbation, the zero-order excitations which absorb light are mainly delocalized single-particle excitons. The small admixture of two-particle excitations has little effect on absorption.[34] For sufficiently large N, periodic boundary conditions can be applied with no loss in accuracy, and each exciton is characterized by a wave vector quantum number, k. To zero-order, excitons are organized into vibronic bands with the $\tilde{v}$th band ($\tilde{v} = 0, 1, ...$) consisting of all single particle excitons with $\tilde{v}$ excited-state vibrational quanta:

$$|k, \tilde{v}\rangle^{(0)} = N^{-1/2}\sum_n \exp(ikn)|n, \tilde{v}\rangle \qquad (4)$$

Only the nodeless $k = 0$ states are optically allowed from the vibrationless ground state, $|G\rangle$.

In H(J)-aggregates, the $k = 0$ exciton in the vth vibronic band, $|A_{v+1}\rangle$, resides at the top (bottom) of the band, see Figure 5a,b. The oscillator strength redistribution observed in Figure 3a,b,f,g is primarily a result of first-order interband coupling between the (zeroth-order) $k = 0$ vibronic excitons in *different* bands (see eq 4), and to a much lesser extent on the coupling between the single- and two-particle excitations as detailed in refs 10 and 33. The result is a diminishing (increasing) value of R_{abs} with W in H(J)-aggregates, where $R_{abs} \equiv I_{A_1}/I_{A_2}$ is the ratio of the oscillator strengths in the A_1 and A_2 bands. In the weak coupling regime, R_{abs} is given by[10,32,33]

$$R_{abs} = \frac{(1 - 0.48J_{k=0}/\omega_0)^2}{(1 + 0.146J_{k=0}/\omega_0)^2} \qquad \lambda^2 = 1, W \ll \lambda^2\omega_0 \quad (5)$$

where the excitonic shift of the $k = 0$ exciton is given by $J_{k=0} = 2J_0$, with $J_{k=0} > 0$ ($J_{k=0} < 0$) in H(J)-aggregates. Equation 5 shows that R_{abs} decreases (increases) upon H(J)-aggregation. A comparison of R_{abs} between isolated and aggregated molecules therefore provides a reliable test for H- or J-type aggregation. Moreover, the exciton bandwidth, $W = 2|J_{k=0}|$, can be obtained from the measured R_{abs}, especially valuable in systems that lack Davydov splitting. Thus far, the attenuation of R_{abs} in H-aggregates has been used to monitor self-assembly in perylene diimide aggregates,[35,36] elucidate the packing arrangement in carotenoid aggregates;[32] and extract the exciton bandwidth and average conjugation lengths in P3HT π-stacks.[10,27,33] The ratio has also been used to establish correlations between the degree and quality of crystallites in P3HT thin films and field-effect transistor characteristics.[26,37]

As W increases into the intermediate and strong excitonic coupling regimes, the spectral centroid continues to shift toward higher energies in H-aggregates and lower energies in J-aggregates. In the strong exciton coupling regime ($W \gg \lambda^2\omega_0$), oscillator strength is mainly concentrated in a single peak due to absorption by a nearly free $k = 0$ exciton with energy of approximately $\omega_{0-0} + D + \lambda^2\omega_0 + 2J_0$ (see Fig. 3e,j). This exciton, labeled as $|H\rangle$ and $|J\rangle$ in the two aggregate types, is created with virtually no change in the ground-state nuclear coordinates; there is essentially no vibronic relaxation subsequent to the vertical excitation because the excitation resonantly jumps to a neighbor before nuclear relaxation can occur. In this regime, the wave functions are approximately Born−Oppenheimer (BO) products of free excitons and phonons,[18,38] where the latter are delocalized 1400 cm^{-1} vibrational excitations defined by a wave vector **q**. Hence, the approximate wave functions are

$$|H\rangle^{(0)} = |J\rangle^{(0)} = \frac{1}{\sqrt{N}}\sum_n |n\rangle \otimes |\mathrm{vac}\rangle \qquad W \gg \lambda^2\omega_0, N \gg 1 \quad (6)$$

where $|\mathrm{vac}\rangle$ indicates the vacuum state for all phonons. Figure 5c,d shows the approximate energy-level diagram in the strong excitonic coupling limit.

We now turn to the photoluminescence spectrum at low temperature. At $T = 0$ K aggregate emission proceeds from the lowest excited state, $|\mathrm{em}\rangle$, with transition energy ω_{em} in accordance with Kasha's rule, which assumes that the exciton lifetime is sufficiently long compared with the inverse spectral diffusion (relaxation) rate induced primarily by exciton−lattice phonon scattering. At 0 K, the "reduced" emission profile takes the form of a vibronic progression,

$$S(\omega) = \sum_{v_t=0,1,2,...} I^{0-v_t}\Gamma(\omega - \omega_{em} + v_t\omega_0) \qquad (7)$$

The spectrum in eq 7 is simplified by excluding the cubic frequency dependence, as well as the frequency-dependent index of refraction, in order to focus on the impact of aggregation on the dimensionless line strengths,

$$I^{0-v_t} = \mu^{-2} \sum_{T(v_t)} |\langle \mathrm{em}|\hat{\mu}|T(v_t)\rangle|^2 \tag{8}$$

The terminal states, $|T(v_t)\rangle$, form a degenerate set of electronic ground states, in which a total of v_t vibrational quanta are distributed over N molecules (this assumes nondispersive or Einstein phonons). Since $\Gamma(0) = 1$, the peak intensities in $S(\omega)$ reflect FC factors in the case of an isolated (single) molecule, with $I_{SM}{}^{0-v_t} = \lambda^{2v_t} \exp(-\lambda^2)/v_t!$.

In ideal H-aggregates composed of *rigid* molecules, oscillator strength is concentrated on top of the free exciton band making the transition from the lowest energy exciton, $|\mathrm{em}\rangle$ (which has $k = \pi$) to the ground state optically forbidden. This was pointed out early on by McCrae and Kasha.[19] In this ideal case, there is no fluorescence, and deexcitation to the ground state must proceed via intersystem crossing or internal conversion. The result follows because the phase of $|\mathrm{em}\rangle$ alternates from molecule to molecule such that the overall aggregate transition dipole moment is effectively canceled out.

In the more physically relevant case of ideal H-aggregates composed of *nonrigid* molecules ($\lambda^2 > 0$), the above scenario no longer holds. In this case, only the 0−0 emission ($|\mathrm{em}\rangle \rightarrow |G\rangle$) is optically forbidden as observed in Figure 3a−e. Sideband emission is allowed because the momentum conservation required in the transition can be maintained by terminating on the ground state with one or more vibrational phonons.[9,38] A missing 0−0 component leads to a decrease in the radiative decay rate since the latter scales with the emission spectral area, $\gamma_{\mathrm{rad}} \propto \int \omega^3 S(\omega)\, d\omega$. Indeed, H-aggregates are known to quench fluorescence in polymer films, making it necessary to prevent aggregation in order to increase the photon yield in organic light-emitting diode (OLED) devices.[39] However, a potentially larger reason for fluorescence quenching in H-aggregates is the dramatic demise in the sideband intensities with increasing exciton bandwidth W as demonstrated in Figure 3a−e. In addition, the 0−1 sideband increasingly dominates the spectrum as W increases. These effects can be understood by appealing to the strong exciton coupling limit where the emitting exciton is approximately the product of a free exciton and the vacuum phonon state. The band-bottom exciton is similar to eq 6 except for the strong phase oscillation characteristic of $k = \pi$ excitons. The lowest energy exciton is approximately given by

$$|\mathrm{em}\rangle^{(0)} = \frac{1}{\sqrt{N}} \sum_n (-1)^n |n\rangle \otimes |\mathrm{vac}\rangle \qquad \begin{matrix}\text{H-agg, } W \gg \lambda^2\omega_0 \\ N \gg 1\end{matrix} \tag{9}$$

First-order vibronic coupling mixes the exciton in eq 9 with states consisting of nodeless excitons with high wave vector phonons ($q = \pi$) near the top of the exciton band, leading to 0−1 emission of the form[40−42]

$$I^{0-1} \approx \frac{\lambda^2 {\omega_0}^2}{(W + \omega_0)^2} \qquad \text{H-agg, } W \gg \lambda^2\omega_0 \tag{10}$$

This expression has been derived in refs 40 and 41 for *ac*-polarized emission in herringbone aggregates but is essentially unaltered for the ideal H-aggregates considered here.

Figure 3a−e also shows that for a given value of W two-particle excitations contribute more to the emission spectrum than to the absorption spectrum. Even for the smallest value of W, there is a significant drop in the emission intensity when two-particle states are included, and this occurs despite the relatively small admixture (0.53%) of two-particle states. Emission is therefore a far more sensitive probe of the polaron radius. Whereas two-particle states *do not* radiatively couple to $|G\rangle$ they *do* couple to vibrationally excited ground states ($|T(v_t)\rangle$ with $v_t \geq 1$) thereby contributing directly to sideband emission (0−1, 0−2, ...). As shown in earlier works,[9,38] the first sideband (0−1) is due to a destructive interference between one- and two-particle emission pathways, which is readily seen by inserting the wave function in eq (1) into the 0−1 line strength in eq (8). As Figure 3 shows, the destructive interference increases with W; for the largest value of W, the 0−1 intensity diminishes by a factor of 3.5 with the inclusion of two-particle states. In distyrylbenzene aggregates with bandwidths approaching 1 eV, the inclusion of the two-particle states leads to a dramatic 20-fold reduction in the *ac*-polarized 0−1 intensity.[38]

Consider now J-aggregate emission. Since the absorption origin is also the emission origin (see Figure 5), there is negligible Stokes shift and the emission band red shifts along with the main absorption band with increasing W, see Figure 3f−j. In contrast to H-aggregates, the emitting exciton has $k = 0$ making the 0−0 emission allowed and enhanced by a factor of N compared with an isolated molecule. This is demonstrated in the inset of Figure 3j. In J-aggregates, the dimensionless intensity of the 0−0 peak,

$$I^{0-0} = |\langle G|\hat{\mu}|\mathrm{em}\rangle|^2/\mu^2 \tag{11}$$

converges to N in the strong excitonic coupling limit where $|\mathrm{em}\rangle$ approaches the nodeless wave function in eq 6. (In Fig-

ure 3, I^{0-0} approaches $0.81N$; the factor of 0.81 reflects open boundary conditions and finite size effects.) The N-fold enhancement arises from a concentration of oscillator strength in the $|\mathrm{em}\rangle \rightarrow |G\rangle$ transition and leads to superradiant decay rates.[8,9,24,28,38,40] More generally, 0−0 emission in J-aggregates is enhanced by the coherence number, N_{coh} ($<N$), which is the number of molecules over which the wave function is coherently spread, as determined by static and dynamic disorder.

In contrast to H-aggregates, the 0−1 peak, observed as a small shoulder in Figure 3f−j, *increases* with W and arises from a *constructive* interference between one- and two-particle coefficients of the emitting exciton. In the limit of very large W where the BO wave functions are accurate zero-order approximations, the 0−1 intensity converges to[42]

$$I^{0-1} = \lambda^2 \qquad \text{J-agg, } W \gg \lambda^2\omega_0 \tag{12}$$

considerably larger than the single molecule value of $\lambda^2\, \mathrm{e}^{-\lambda^2}$. More importantly, the 0−1 intensity is *not* coherently enhanced by N_{coh} in either J- or H-aggregates. The inset of Figure 3j shows that despite a 4-fold increase in N, the 0−1 sideband intensity remains essentially constant. Thus arises a very fortunate situation: the ratio of the 0−0 to 0−1 line strengths, R_{em}, provides a direct measure of N_{coh}. In the limit of $W \gg \lambda^2\omega_0$, R_{em} is simply N/λ^2 in ideal J-aggregates, where $N_{\mathrm{coh}} = N$. The linear dependence of R_{em} on N_{coh} is quite general for any aggregate morphology in which the 0−0 transition is dipole allowed. For example, in $(\mathrm{OPV})_n$ and $(\mathrm{OT})_n$ (n even) herringbone aggregates, the 0−0 transition is weakly allowed due to a slight misalignment of the transition dipole moment with the long molecular axis. In this case, the ratio of the *b*-polarized 0−0 peak to the mainly *ac*-polarized first sideband gives N_{coh}, which is determined by disorder and temperature.[9,40,41] (The ratio involving the *b-polarized* sideband also scales with N_{coh}.[42]) Another example is the intrinsic emission from thin films of anthracene[29] and tetracene[30] in which the lower Davydov component is strongly allowed, yielding an intense 0−0 origin followed by a much weaker sideband. This is demonstrated in Figure 6, which shows early time emission spectra for vacuum-deposited tetracene films. Analysis of R_{em} leads to a coherence number of approximately 10 at $T = 4$ K.

The determination of the coherence number from the PL spectral line shape is an alternative to the more established means of obtaining N_{coh} from the superradiant decay rate or an analysis of the nonlinear absorption line shape.[43,44] One important advantage of the PL technique is that R_{em} is insensitive to nonradiative decay processes, which serve only to attenuate the PL spectrum uniformly. R_{em} is, however, sensitive to self-absorption, which must be carefully eliminated by using optically thin samples or collecting front face emission.[25] Finally, intrinsic exciton emission may require early time collection,[29,30] before low-energy traps (chemical impurities and structural defects[9]) can be populated.

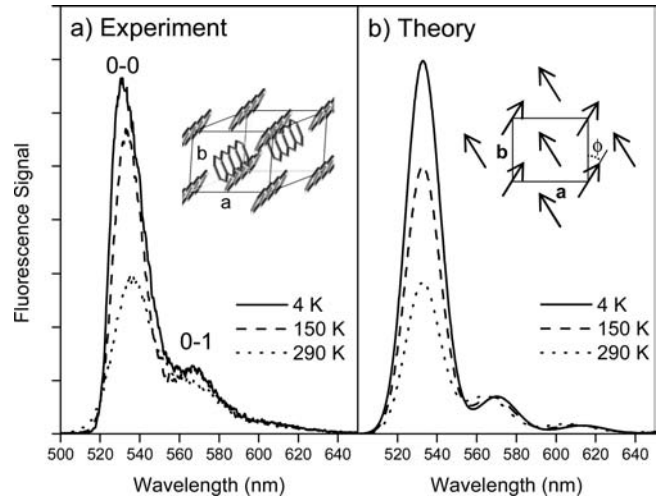

FIGURE 6. (a) Photoluminescence spectrum from vacuum-deposited tetracene films integrated over the first 50 ps from ref 30. (b) Theoretical spectrum using one- and two-particle states. Reprinted with permission from ref 30. Copyright 2009 by the APS.

IV. Static Disorder and Thermal Effects

In this section, we focus on the effect of site-energy disorder and increasing temperature on ideal H- and J-aggregate emission. The impact of disorder on the absorption spectral line widths including motional narrowing has already been covered in great detail.[45,46] We also omit any discussion surrounding the temperature-dependent homogeneous line width and focus entirely on the emission line strengths, with $I^{0-\nu_t}$ identified with the spectral *area* of the $0-\nu_t$ peak.

Figures 7 and 8 show how $S(\omega)$ changes with increasing disorder and temperature for the aggregates in Figure 3b,g with $W = \lambda^2\omega_0$. We averaged over 10^3 configurations of transition frequency offsets, Δ_n, chosen randomly from a Gaussian distribution,

$$P(\Delta_n) = (\sqrt{\pi}\sigma)^{-1} \exp(-\Delta_n{}^2/\sigma^2) \tag{13}$$

with inhomogeneous line width, σ. As demonstrated in Figure 7, site-energy (diagonal) disorder breaks the symmetry allowing 0−0 emission in H-aggregates.[10−12] Disorder in the electronic couplings has the same effect, although a quantitative analysis of off-diagonal disorder on the vibronic progression has yet to be made. In Figure 7a, the integrated sideband emission also increases with σ, albeit at a far smaller rate. By contrast in J-aggregates the 0−0 intensity decreases

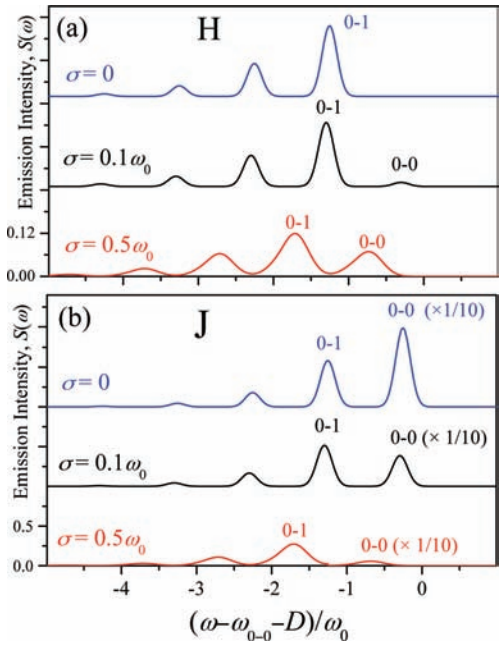

FIGURE 7. Calculated H- and J-aggregate emission spectra as a function of increasing site disorder at $T = 0$ K for linear aggregates with $N = 20$ chromophores. In all panels, $D = 0$, $W = \lambda^2\omega_0$, $\lambda^2 = 1$, $\omega_0 = 0.17$ eV, and $\sigma_{hom} = 0.14\omega_0$. Note that *only* the 0−0 peak in panel b is reduced by a factor of 10 (side bands are not rescaled).

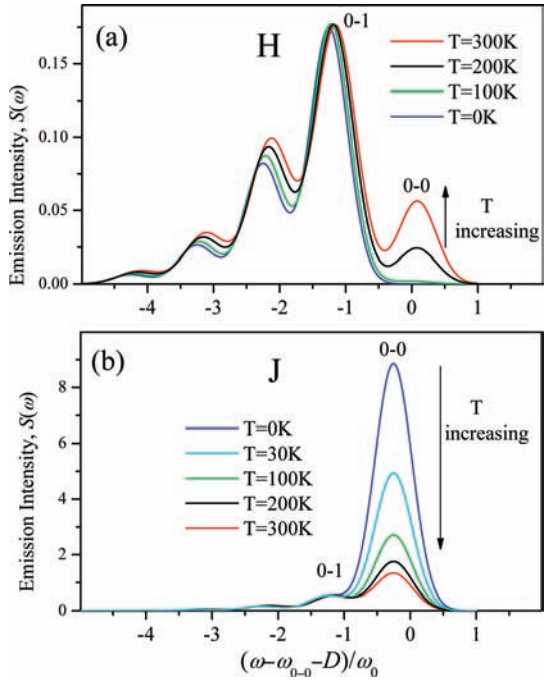

FIGURE 8. Calculated disorder-free H- and J-aggregate emission spectra as a function of temperature for linear aggregates with $N = 20$, calculated by averaging over a Boltzmann distribution of emitters. In all panels, $D = 0$, $W = \lambda^2\omega_0$, $\lambda^2 = 1$, $\omega_0 = 0.17$ eV, and $\sigma_{hom} = 0.4\omega_0$.

markedly (while the sideband intensities decrease slightly) with increasing σ, as N_{coh} is reduced below N due to localization. Hence, the ratio $R_{em} \equiv I^{0-0}/I^{0-1}$, increases (decreases) with increasing disorder in ideal H(J)-aggregates. In the limit of extreme disorder, $S(\omega)$ for both aggregate types approaches a broad, isolated-molecule spectrum with $R_{em} \rightarrow 1/\lambda^2$.

In both aggregate types, 0−0 emission is a strong function of N_{coh}, in marked contrast to the sidebands.[11,29,38] In ideal H-aggregates, the absence of the 0−0 peak indicates that $N_{coh} = N$, but, unlike in J-aggregates, the interference is totally destructive. When disorder is absent, the coherence function for the emitting exciton[11,47] oscillates like $(-1)^n$ over the entire H-aggregate leading to a complete cancellation of the 0−0 transition moment. In J-aggregates, the coherence function has the same spatial envelope but with no nodes (since $k = 0$), creating a constructive interference. As N_{coh} shrinks with increasing disorder, R_{em} therefore increases (decreases) in H(J)-aggregates. Recently, N_{coh} was derived from the measured R_{em} in mono-functionalized OPV[47,48] and P3HT[11] H-aggregates. Detailed analysis of the emission spectral shape and Stokes shift using spatially correlated disorder also allowed for a crude determination of the incoherent exciton migration length, the extent to which energy can hop between coherent domains.[11,48]

We next consider thermal effects on the intrinsic exciton emission. The analysis is simplified by omitting thermally activated trap states and possible competition from excimer emission. We focus entirely on the effect of temperature on the line strengths, and omit the T-dependent broadening due to scattering with lattice phonons. The spectra in Figure 8 were evaluated by averaging over a Boltzmann distribution of emitting excitons.

As observed in Figure 8, increasing temperature leads to enhanced 0−0 emission in H-aggregates and the opposite behavior in J-aggregates. The former effect is due to thermally activated emission from the dipole-allowed $k = 0$ exciton, $|A_1\rangle$ (see Figure 5a), which is $\sim e^{-\lambda^2} W$ above the band bottom. In J-aggregates, the demise of the 0−0 emission with T derives from the fact that thermally excited excitons with $k \neq 0$ cannot emit to the vibrationless ground state but *can emit* to vibrationally excited electronic ground states. The effect can be described in terms of a thermal coherence size, N_T ($<N$), which has an activated temperature dependence when N or T are small enough so that kT is smaller than the exciton level separations but turns over to[40,41]

$$N_T = 1 + 4\pi\omega_c/(kT) \qquad (14)$$

in the thermodynamic limit, where ω_c is the curvature of the exciton band-bottom.[40,41] Since $N_T < N$, superradiance can be strongly quenched with increasing T.[40,41] The theory also pre-

dicts temperature-independent sideband line strengths as observed in Figure 8, so that N_T can be obtained directly from R_{em}. The temperature dependence of $S(\omega)$ applies not only to ideal *J*-aggregates but to any morphology in which the 0−0 transition is dipole allowed, including the herringbone packing found in oligothiophene,[22,40,41] anthracene,[29] and tetracene[30] thin films. Finally, when temperature is increased in *disordered* aggregates, the effect on R_{em} is qualitatively similar to that in disorder-free aggregates.[11,41] In this case, R_{em} responds to a coherence number, N_{coh}, defined by both the magnitude of disorder and temperature.

V. Discussion and Conclusion

The multiparticle representation of Hamiltonians describing exciton−vibrational coupling in organic assemblies provides an excellent starting point for evaluating the fundamental excitations responsible for the optical response. Such excitations are polaronic Frenkel excitons in which a central *vibronic* excitation is surrounded by a field of *vibrational* excitations. The latter are accounted for by two-particle excitations and play an essential role in the absorption and emission spectral line shapes.

The manner in which the FC progression based on the ubiquitous vinyl stretching mode in conjugated molecules is distorted upon aggregation allows one to determine the exciton bandwidth, the coherence number, and parameters describing disorder. Ideal H- and J-aggregates represent the two extremes in the FC distortion: in H(J)-aggregates, the vibronic peak ratio R_{abs} decreases (increases) with exciton bandwidth W, while R_{em} increases (decreases) with increasing disorder and rising temperature. These contrasting behaviors establish a basis for analyzing the photophysical response in more complex morphologies. For example, lutein diacetate aggregates, which were formerly thought to be J-like based on spectral shifts, are actually H-like, with R_{abs} significantly decreasing with aggregation.[32] Moreover, in packing arrangements with multiple molecules in a unit cell, oscillator strength generally occurs in the top and bottom of the exciton band, leading to optical properties that contain elements of both ideal J- and H-aggregate behavior, depending upon the polarization. An interesting example is provided by $(OPV)_n$ and $(OT)_n$ crystals[22] in which most of the oscillator strength resides near the top of the band, yielding a dominant H-like *ac*-polarized absorption profile. Emission from the weakly allowed band-bottom contains both *ac*- and *b*-polarized components, resembling ideal H- and J-aggregate emission, respectively. Furthermore, because the 0−0 transition is so weak, $(OPV)_n$ and $(OT)_n$ aggregates require a threshold[8,22] in N_{coh} to realize superradiance,[28] in marked contrast to polyacene crystals.[29,30]

Sideband photoluminescence is particularly sensitive to two-particle states due to a destructive (constructive) interference between one- and two-particle emission pathways in H(J)-aggregates. An ideal background-free measure of the two-particle contribution, and therefore the polaron radius, is provided by circularly polarized luminescence in chiral aggregates, where the sideband dissymmetry scales directly with the two-particle coefficients.[47]

Finally, the coupling to additional lower-energy vibrational modes beyond the symmetric stretching mode can lead to interesting intermode synergistic effects.[42,49] Because low-energy modes ($\lesssim$500 cm^{-1}) are better described under the BO approximation, a more robust theory for the photophysical response of organic assemblies involves a polaron−phonon basis set.[50] We are currently exploring further the intricacies of multiple mode coupling.

F.C.S. is supported by the NSF, Grant DMR-0906464.

BIOGRAPHICAL INFORMATION

Frank C. Spano (Ph.D. Physical Chemistry, Princeton University, 1988) is a professor in the Department of Chemistry, Temple University. His research involves theoretical modeling of excited states in organic materials.

FOOTNOTES

*E-mail: spano@temple.edu.

REFERENCES

1 Forrest, S. R. The path to ubiquitous and low-cost organic electronic appliances on plastic. *Nature* **2004**, *428*, 911–918.
2 Gunes, S.; Neugebauer, H.; Sariciftci, N. S. Conjugated polymer-based organic solar cells. *Chem. Rev.* **2007**, *107*, 1324–1338.
3 Friend, R. H.; Gymer, R. W.; Holmes, A. B.; Burroughes, J. H.; Marks, R. N.; Taliani, C.; Bradley, D. D. C.; Santos, D. A. D.; Bredas, J. L.; Logdlund, M.; Salaneck, W. R. Electroluminescence in conjugated polymers. *Nature* **1999**, *397*, 121–128.
4 Heeger, A. J. Nobel Lecture: Semiconducting and metallic polymers: The fourth generation of polymeric materials. *Rev. Mod. Phys.* **2001**, *73*, 681–700.
5 Toyozawa, Y. Self-Trapping of an Electron by the Acoustical Mode of Lattice Vibration. I. *Prog. Theor. Phys.* **1961**, *26*, 29–44.
6 Levinson, Y. B.; Rashba, E. I. Electron-phonon and exciton-phonon bound states. *Rep. Prog. Phys.* **1973**, *36*, 1499–1565.
7 Holstein, T. Polaron motion. I. Molecular-crystal model. *Ann. Phys.* **1959**, *8*, 325–342.
8 Spano, F. C. Emission from aggregates of oligo-phenylene vinylenes: A recipe for superradiant H-aggregates. *Chem. Phys. Lett.* **2000**, *331*, 7–13.
9 Spano, F. C. Absorption and emission in oligo-phenylene vinylene nanoaggregates: the role of disorder and structural defects. *J. Chem. Phys.* **2002**, *116*, 5877–5891.
10 Spano, F. C. Modeling disorder in polymer aggregates: The optical spectroscopy of regioregular poly(3-hexylthiophene) thin films. *J. Chem. Phys.* **2005**, *122*, 234701. *J. Chem. Phys.* **2007**, *126*, 159901.

11 Spano, F. C.; Clark, J.; Silva, C.; Friend, R. H. Determining exciton coherence from the photoluminescence spectral line shape in poly(3-hexylthiophene) thin films. *J. Chem. Phys.* **2009**, *130*, 074904.

12 Meskers, S. C. J.; Janssen, R. A. J.; Haverkort, J. E. M.; Wolter, J. H. Relaxation of photo-excitations in films of oligo- and poly-(para-phenylene vinylene) derivatives. *Chem. Phys.* **2000**, *260*, 415–439.

13 Stradomska, A.; Petelenz, P. Intermediate vibronic coupling in sexithiophene single crystals. *J. Chem. Phys.* **2009**, *130*, 094705.

14 Eisfeld, A.; Briggs, J. S. The J- and H-bands of organic dye aggregates. *Chem. Phys.* **2006**, *324*, 376–384.

15 Hoffmann, M.; Soos, Z. G. Optical absorption spectra of the Holstein molecular crystal for weak and intermediate electronic coupling. *Phys. Rev. B* **2002**, *66*, 024305.

16 Seibt, J.; Engel, V. Absorption and emission spectroscopy of molecular trimers: Cyclic versus linear geometries. *Chem. Phys.* **2008**, *347*, 120–126.

17 Philpott, M. R. Theory of coupling of electronic and vibrational excitations in molecular crystals and helical polymers. *J. Chem. Phys.* **1971**, *55*, 2039–2054.

18 Kasha, M. Energy Transfer Mechanisms and the Molecular Exciton Model for Molecular Aggregates. *Radiat. Res.* **1963**, *20*, 55–70.

19 McRae, E. G.; Kasha, M. Enhancement of phosphorescence ability upon aggregation of dye molecules. *J. Chem. Phys.* **1958**, *28*, 721–722.

20 This assumes that the wave function phases are chosen so that the in-phase combination corresponds to transition dipole moments pointing in a common direction.

21 Oelkrug, D.; Egelhaaf, H.-J.; Gierschner, J.; Tompert, A. Electronic deactivation in single chains, nano-aggregates and ultrathin films of conjugated oligomers. *Syn. Met.* **1996**, *76*, 249–253.

22 Spano, F. C. Excitons in conjugated oligomer aggregates, films, and crystals. *Annu. Rev. Phys. Chem.* **2006**, *57*, 217–243.

23 *J-aggregates*; Kobayashi, T., Ed.; World Scientific: Singapore, 1996, p 228.

24 Fidder, H.; Knoester, J.; Wiersma, D. A. Superradiant emission and optical dephasing in J-aggregates. *Chem. Phys. Lett.* **1990**, *171*, 529–536.

25 Brown, P. J.; Thomas, S. D.; Kohler, A.; Wilson, J. S.; Kim, J.-S.; Ramsdale, C. M.; Sirringhaus, H.; Friend, R. H. Effect of interchain interactions on the absorption and emission of poly(3-hexylthiophene). *Phys. Rev.B* **2003**, *67*, 064203.

26 Clark, J.; Chang, J. F.; Spano, F. C.; Friend, R. H.; Silva, C. Determining exciton bandwidth and film microstructure in polythiophene films using linear absorption spectroscopy. *Appl. Phys. Lett.* **2009**, *94*, 163306.

27 Clark, J.; Silva, C.; Friend, R. H.; Spano, F. C. Role of intermolecular coupling in the photophysics of disordered organic semiconductors: Aggregate emission in regioregular polythiophene. *Phys. Rev. Lett.* **2007**, *98*, 206406.

28 Meinardi, F.; Cerminara, M.; Sassella, A.; Bonifacio, R.; Tubino, R. Superradiance in Molecular H Aggregates. *Phys. Rev. Lett.* **2003**, *91*, 247401.

29 Ahn, T. S.; Muller, A. M.; Al-Kaysi, R. O.; Spano, F. C.; Norton, J. E.; Beljonne, D.; Bredas, J. L.; Bardeen, C. J. Experimental and theoretical study of temperature dependent exciton delocalization and relaxation in anthracene thin films. *J. Chem. Phys.* **2008**, *128*, 054505.

30 Lim, S.-H.; Bjorklund, T. G.; Spano, F. C.; Bardeen, C. J. Exciton delocalization and superradiance in tetracene thin films and nanoaggregates. *Phys. Rev. Lett.* **2004**, *92*, 107402.

31 Zsila, F.; Bikadi, Z.; Keresztes, Z.; Deli, J.; Simonyi, M. Investigation of the self-organization of lutein and lutein diacetate by electronic absorption, circular dichroism spectroscopy, and atomic force microscopy. *J. Phys. Chem. B* **2001**, *105*, 9413–9421.

32 Spano, F. C. Analysis of the UV/vis and CD spectral line shapes of carotenoid assemblies: Spectral signatures of chiral H-aggregates. *J. Am. Chem. Soc.* **2009**, *131*, 4267–4278.

33 Spano, F. C. Absorption in regioregular poly(3-hexylthiophene) thin films: Fermi resonances, interband coupling and disorder. *Chem. Phys.* **2006**, *325*, 22–35.

34 In order to simplify the discussion, we omit the zero-order mixing between degenerate one- and two-particle states, which leads to small spectral splittings not resolvable in Figure 3. For details, see ref 33.

35 Shaller, A. D.; Wang, W.; Gan, H. Y.; Li, A. D. Q. Tunable molecular assembly codes direct reaction pathways. *Angew. Chem., Int. Ed.* **2008**, *47*, 7705–7709.

36 Dehm, V.; Chen, Z. J.; Baumeister, U.; Prins, P.; Siebbeles, L. D. A.; Wurthner, F. Helical growth of semiconducting columnar dye assemblies based on chiral perylene bisimides. *Org. Lett.* **2007**, *9*, 1085–1088.

37 Chang, J. F.; Clark, J.; Zhao, N.; Sirringhaus, H.; Breiby, D. W.; Andreasen, J. W.; Nielsen, M. M.; Giles, M.; Heeney, M.; McCulloch, I. Molecular-weight dependence of interchain polaron delocalization and exciton bandwidth in high-mobility conjugated polymers. *Phys Rev. B* **2006**, *74*, 115318.

38 Spano, F. C. The fundamental photophysics of conjugated oligomer herringbone aggregates. *J. Chem. Phys.* **2003**, *118*, 981–994.

39 Schwartz, B. J. Conjugated polymers as molecular materials: How chain conformation and film morphology influence energy transfer and interchain interactions. *Annu. Rev. Phys. Chem.* **2003**, *54*, 141–172.

40 Spano, F. C. Temperature dependent exciton emission from herringbone aggregates of conjugated oligomers. *J. Chem. Phys.* **2004**, *120*, 7643−7658. *J. Chem. Phys.* **2004**, *121*, 5555.

41 Spano, F. C. Temperature dependent emission in disordered herringbone aggregates of conjugated oligomers. *Phys. Rev. B* **2005**, *71*, 235208.

42 Zhao, Z.; Spano, F. C. Multiple mode exciton-phonon coupling: applications to photoluminescence in oligothiophene thin films. *J. Phys. Chem. C* **2007**, *111*, 6113–6123.

43 Dahlbom, M.; Pullerits, T.; Mukamel, S.; Sandstrom, V. Exciton delocalization in the B850 light-harvesting complex: Comparison of different measures. *J. Phys. Chem. B* **2001**, *105*, 5515–5524.

44 Bakalis, L. D.; Knoester, J. Pump-probe spectroscopy and the exciton delocalization length in molecular aggregates. *J. Phys. Chem. B* **1999**, *103*, 6620–6628.

45 Knapp, E. W. Lineshapes of molecular aggregates. Exchange narrowing and intersite correlation. *Chem. Phys.* **1984**, *85*, 73–82.

46 Knoester, J. Nonlinear optical line shapes of disordered molecular aggregates: motional narrowing and the effect of intersite correlations. *J. Chem. Phys.* **1993**, *99*, 8466–8479.

47 Spano, F. C.; Meskers, S. C. J.; Hennebicq, E.; Beljonne, D. Probing excitation delocalization in supramolecular chiral stacks by means of circularly polarized light: experiment and modeling. *J. Am. Chem. Soc.* **2007**, *129*, 7044−7054. *J. Am. Chem. Soc.* **2007**, *129*, 16278.

48 van Dijk, L.; Bobbert, P. A.; Spano, F. C. Optical spectra and Stokes shift in double-stranded helical supramolecular assemblies. *J. Phys. Chem B* **2009**, *113*, 9708–9717.

49 Silvestri, L.; Tavazzi, S.; Spearman, P.; Raimondo, L.; Spano, F. C. Exciton-phonon coupling in molecular crystals: Synergy between two intramolecular vibrational modes in quaterthiophene single crystals. *J. Chem. Phys.* **2009**, *130*, 234701.

50 Zhao, Z.; Spano, F. C. Vibronic fine structure in the absorption spectrum of oligothiophene thin films. *J. Chem. Phys.* **2005**, *122*, 114701.